Multiscale Green's functions for modeling of nanomaterials: Bridging length and time scales[1]

V.K. Tewary

Applied Chemical and Materials Division,

National Institute of Standards and Technology, Boulder, CO 80305, USA

(Keywords (alphabetical order): extending time scales; graphene; lattice statics; linking length scales; multiscale Green's functions.)

Abstract

Green's function gives the response of a system to a probe and is a powerful technique for solving a variety of problems in science and engineering. We describes a multiscale Green's function method for modeling nanomaterials at different length and time scales. In the static case the method can seamlessly link the length scales from atomistic to continuum in an integrated formalism. In time-dependent problems, this method can simulate physical processes in a multipartcle system over a wide range extending from femto seconds to micro seconds within a reasonable CPU time. For illustration, the method is applied to simulate elastic deformation and propagation of elastic waves in two-dimensional graphene.

1. Introduction

Fabrication and analysis of nanostructures and new nanomaterials have been growing exponentially over the last few years (see, for example, the papers quoted in this volume). However, to advance the nanotechnology in a systematic way, it is absolutely vital that robust and reliable mathematical models are available. In fact, materials modeling has now emerged as a new branch of knowledge that has tremendous scientific and industrial applications. These models help in the visualization of materials and understanding of the physical processes at length and time scales that are difficult and indeed expensive to explore by direct experimental methods. The models are therefore useful for scientific research as well as pedagogical purposes. Moreover, they are indispensable tools for industry for designing and testing of new materials because they can provide quick and inexpensive answers to 'what if' type questions and can give an estimate of the lifetime and reliability of the materials for different applications and under different operating conditions. Modeling supported by data is the basis of the materials genome initiative, a major new research initiative being pursued in the USA.

In this chapter we describe a Green's function (GF) method for multiscale modeling nanomaterials and nanostructures. Green's function is a well-established technique for solving a variety of problems in science and engineering [1], [2]. The application of the GFs to phonons in a lattice is given in the excellent treatise by Maradudin et. al [3]. The static GF, which is the zero frequency limit of the phonon GF, has been described in an earlier paper [4]. The GF techniques have been extensively applied in the continuum model of a solid as described in a very good book by Ting [5]. These techniques have

contributed to the multiscale Green's function (MSGF) method described in this chapter for the nanomaterials.

The plan of the chapter is as follows: The present section, Sec. 1 is the introduction. The rest of this section gives the need for multiscale modeling – for bridging length and time scales, and for its application to graphene. The basic GF technique is described in Sec. 2. A review of the lattice model of a solid as relevant for lattice GFs is given in Sec. 3 and the lattice statics Green's function (LSGF) is described in Sec. 4. The MSGF method for length and time scales are described in Sec. 5 and 6 respectively. Finally, the application of the MSGF method for graphene is presented in Sec. 7.

1.1 Need for bridging length scales

The challenges associated with the modeling of nanostructures arise due to the fact that the material system usually contains "defects" at various length scales: (i) the core region of the nanostructure and lattice defects at the atomistic scale(sub-nano regime) where nonlinear effects may be important, (ii) free surfaces in the nanostructure and its interface with the host solid and the region of the host solid around the nanostructure (nano regime), and (iii) free surfaces and interfaces (with thin films) in the host solid (macro regime). It is therefore necessary that a model for nanostructures links not only the nano and macro regimes but also the sub-nano regime. It has to be an integrated model in which each length scale seamlessly merges into the next scale.

Lattice defects can be classified in two broad categories- potential defects and structural defects. The potential defects are those that can be simulated by a change in the potential

energy or the Hamiltonian of the crystal. Examples of potential defects are point defects such as vacancies and interstitials or their aggregates such as voids, precipitates, hillocks, etc. In contrast, the structural defects or extended defects consist of major rearrangements of atoms in the lattice and cannot be represented by a change in the crystal Hamiltonian alone. Examples of structural defects are dislocations, free surfaces, interfaces, etc. These defects affect the mechanical properties of all solids but are especially important for nanostructures because they can strongly degrade the functional performance of the nanostructure in many cases, for example, its interaction with light.

For ordinary macroscopic solids lattice defects can be adequately modeled by using the anisotropic continuum theory which can be used to calculate the stresses and strains in the solid. These two are the most important measurable parameters that characterize the mechanical behavior of a solid and are mutually related by the elastic constants of the solid. It is also necessary to account for piezoelectric effects and electric polarization effects associated with certain materials; this can be done by using the continuum model.

Free surfaces and interfaces play a relatively large role in nanomaterials as compared to their role in ordinary solids. Many physical properties of nanomaterials and nanostructures in thin films depend upon the strains near the free surfaces and the interfaces caused by point defects. For example, the formation of quantum dots and their arrays depends strongly upon the strains near the free surface of the substrate. Optical and electronic properties of quantum dots are also sensitive to strains. Electromigration in copper interconnects and the efficiency of GaN and other III-V LED devices depend upon the concentration profile of vacancies and other point defects.

It is generally accepted that the continuum theory is inadequate to describe the response of a crystal lattice close to a defect [4]. This region in which the continuum model is not valid extends from sub-nano to a few nanometers. It then becomes necessary to model the discrete atomistic structure of the lattice in this region. On the other hand the continuum theory is adequate to model the response of the solid at sufficiently large distances from the defects and is also adequate to model free surfaces and interfaces that are not too close to the point defects. At the macroscopic level the continuum theory is a highly developed theory that has been very successful in modeling the macroscopic response of solids and for interpreting measurements of stresses and strains that are essentially the continuum model parameters. The problem is that the physical processes that determine the macroscopic stresses and strains, in particular, the energetics of interatomic displacements, occur at the atomistic or sub-nano scales . Hence a multiscale model is needed to relate the physical processes to macroscopic parameters for the purpose of design and interpretation of measurements that are sensitive to atomic-scale phenomena.

Further, for reasons described earlier, the atomistic arrangements inside and around a nanostructure (its interface with the host solid) and near the point defects have to be modeled by using a discrete-lattice theory. On the other hand, those regions of the free surfaces and the interfaces which are distant from the nanostructures and the point defects can be modeled by using the continuum theory. In fact for structural applications the continuum theory may be preferable for modeling such regions. A pure lattice-theory model of the macroscopic free surfaces and interfaces of the host lattice is difficult because of uncertain factors like surface reconstruction, presence of impurities, and a lack of knowledge of reliable interatomic potentials near the surface [6]. The interatomic

potentials which may be reliable in the bulk of the solid may not be valid at or close to the surface because of factors like electronic rearrangements. On the other hand, the continuum model gives at least a reasonably correct macroscopic representation of structural defects [7], which has been verified experimentally over the last several years. Moreover, measurements of the strains are mostly made at or near a free surface. Since strain is a continuum parameter, it is convenient to represent the free surfaces of the host solid away from the defect by using the continuum model.

1.2 Bridging the time scales

A large class of materials modeling problems deal with the simulation and understanding of time dependent processes. Examples are diffusion, phonon transport, thermal conduction, crack propagation, radiation damage, and many more. Presently various non-silicon materials such as carbon nanotubes and graphene are being considered as adjuncts or additions to the CMOS technology and other semiconductor applications. A huge amount of work has been published on temporal processes in conventional materials but not so much on graphene, nanotubes, and other nanomaterials. This is partly because the continuum model and the analytical and semi-analytical formulae work reasonably well for bulk materials but not for nanomaterials that must be simulated at the atomistic scales.

To appreciate the problem of temporal modeling and the need to bridge the time scales, we consider radiation damage in solids as an example. Because of the obvious difficulties associated with the purely experimental investigation of the nanoscale phenomena, even

more so when radiation damage is involved, it is necessary to develop reliable mathematical models for the effect of radiation on the new nanomaterials.

Radiation damage often results in lattice displacements (see, for example, [8]) that lead to the creation of vacancies and interstitials (primary event). These lattice changes can agglomerate into clusters and, under certain conditions, form voids and hillocks/dislocations (secondary and higher events). They may also get distributed randomly to make the crystal amorphous. The charge distribution in the crystal is strongly perturbed due to the lattice defects, which may cause the device to fail. In order to model the reliability and performance of the device when exposed to high-energy radiation, it is, therefore, necessary to track the movement of vacancies and interstitials and determine the conditions under which they aggregate or settle randomly. A precise knowledge of atomic locations is also needed for calculating charge distribution and other processes such as transport of hydrogen in graphene and nanotubes that are important for estimating the reliability of those devices.

Radiation damage is just one of many physical processes where bridging time scales is crucial. The most challenging aspect of modeling these processes is that the primary event occurs over femtoseconds, whereas the accumulation of defects and other secondary events occur over several nano or even microseconds. It is therefore necessary to develop models that can bridge the time scales from femto to microseconds.

Atomistic modeling of materials and physical processes is presently done by use of molecular dynamics (MD) and its variations [9]. A major stumbling block in classical as well as *ab initio* MD is the extremely limited time scale. Convergence requirements limit

the time step in MD analysis to a few femtoseconds in most materials. In some idealized cases, the time step can be extended to at most a few picoseconds by using very elegant techniques [10]. Still it would require 10^6-10^9 time integration steps in the conventional MD analysis to model material processes at time scales of practical interest (nano to micro seconds). This is a formidable task even for modern computers but has been a long-sought goal. We will describe here a mathematical technique that is a hybrid of causal GF and MD, which can accelerate the temporal convergence by several orders of magnitude [11].

1.3 Application

We will illustrate the MSGF method by applying it to graphene for bridging the length scales as well as the temporal scales. Graphene is a 2D hexagonal lattice of covalently bonded carbon atoms [12]. It is widely regarded as having a strong potential for application in revolutionary new devices [13]. In order to develop graphene-based devices, an important requirement is to control the local curvature of graphene films. This would require an understanding of the mechanical deflection of graphene and to develop techniques for its multiscale modeling ranging from the atomistic to the device level.

It has been only a few years since graphene was invented/discovered. In spite of its short history, so much of work has been published on graphene that it is not treated as a new material anymore. In fact many more 2D materials have now been identified that may be even more promising than graphene like boron nitride, molybdenum disulfide, silicene, phosphorene, etc. [14, 15] . It is apparent that a whole new class of materials is emerging that have the potential to revolutionize the materials industry. Still, graphene remains the

main prototype of this new class of materials because of the simplicity of its structure and very fascinating electronic and mechanical properties. The importance of understanding graphene therefore cannot be overemphasized.

The MSGF can be used to model the mechanical strength of graphene, which should be useful for developing, for example, flexible electronic devices. The temporal modeling is useful for developing new methods of characterizing graphene samples and understanding processes like propagation of ripples [16] that play an important role in the stability of graphene.

2. Green's function method- the basics

In any scientific measurement process, we measure the response of a system to a probe. The mathematical function that defines the response is called the response function and is a characteristic of the system. We need to know the physical process that determines this function. The physical process is represented in terms of an equation or a mathematical relationship which may be an algebraic, differential, or an integral equation. The equation needs to be solved to obtain the response function. In general the objective of modeling is to calculate this function which will enable us to predict the response of the system to a probe. Green's function is essentially the response function of a system. Obviously the choice of the GF would depend upon the nature of the response that we are trying to model.

We can write symbolically the following equation, which is the master equation for all scientific measurements:

Response = Response function * Probe (1)

The so called forward problem is when the response function and the probe are known and we want to find the response. The inverse problem is when the probe and the response are known and we want to obtain the response function.

For example, consider a simple experiment on a particle of mass m attached at the end of a massless spring of spring constant ϕ. The spring is attached to a wall as shown in Fig. 1. We apply a force f on the spring and measure u, the displacement of the end of the spring. The physical process that gives the displacement of the point A is expressed in the terms of the following simple equation

$$f = \phi u, \qquad (2)$$

In this example, the applied force f is the probe and u, the displacement of the particle, is the response of the spring. In this one-dimensional (1D) case, f,u, and ϕ are all scalars. In general they are vectors and tensors. In this chapter our interest is mainly in the calculation of the particle displacements in a multiparticle system. The displacement field, that gives the displacement of each particle, is the most important field quantity for modeling of elastic and thermal characteristics of a material system. Most of the elastic and thermal parameters of a material such as stress and strain, heat diffusion etc., require calculation of the particle displacements.

We can write the solution of Eq. (2) as

$$u = G f \qquad (3)$$

where $G = 1/\phi$. In Eq. (3) G is the GF that gives the response of the spring to the applied probe f. Notice that G is independent of both f and u and is solely a characteristic of the spring. If we know G, we can obtain displacement for any applied force.

The GF obtained above is the static GF in contrast to the dynamic GF that is used for time dependent problems. Now let us expand our example to include the time dependence. Suppose the probe is an applied force that is a function of time t. The equation of equilibrium in this case is given by

$$\phi u + M \partial^2 u/\partial t^2 = f(t), \qquad (4)$$

where m is the mass of the particle A. We write Eq. (4) in the form of a linear operator equation as follows:

$$Pu(t) = f(t) \qquad (5)$$

where the operator P is defined as

$$P = (\phi + m\, \partial^2/\partial t^2) \qquad (6)$$

The formal solution of Eq. (5) is given by

$$u(t) = P^{-1} f = Gf(t) \qquad (7)$$

where

$$G = P^{-1} \qquad (8)$$

We identify G as the GF that is the inverse of the operator P. It is the particular solution of the equation

$$P_t\, G(t,t') = \delta (t-t'), \qquad (9)$$

where t' is also a time variable in the same space as t but is independent of t, and δ (t) is the Dirac delta function which is zero for a nonzero argument. The delta function in Eq. (9) is defined by the following well-known integral relationship:

$$Z(t) = \int \delta (t-t') Z(t') dt', \qquad (10)$$

where Z(t) is any arbitrary but integrable function of t and the integration is over all t-space. The subscript at P in Eq. (9) indicates that it operates only on the variable t and not on t'. We can now write the formal solution given by Eq. (7) in the following general form

$$u(t) = \int G (t-t') f(t') dt', \qquad (11)$$

where the integration is over all t-space. It can be easily verified that Eq. (11) is the solution of Eq. (5) by substitution and using Eqs. (9) and (10). Note that we have written G as a function of single argument t-t' which assumes that G depends upon t and t' only through their difference.

Now we derive an expression for G. We note that it is an operator so we need a representation for G. Let us try the Fourier representation and express all quantities in terms of their Fourier transforms defined as follows:

$$f(t) = (1/2\pi)\int f(\omega) \exp(\iota\omega t) d\omega, \qquad (12)$$

$$u(t) = (1/2\pi)\int u(\omega)\exp(\iota\omega t)\, d\omega, \qquad (13)$$

and

$$G(t) = (1/2\pi)\int G(\omega)\exp(\iota\omega t)\, d\omega, \qquad (14)$$

where ω is the variable conjugate to t and $\iota = \sqrt{-1}$. The integration in Eqs (12)-(14) is over all ω space. We now specify that both the variables t and ω range from $-\infty$ to $+\infty$.

The delta function has the following Fourier representation [2]

$$\delta(t) = (1/2\pi)\int_{-\infty}^{\infty} exp(\iota wt)\, d\omega. \qquad (15)$$

From Eq. (15) we can obtain the inversion relationship for the Fourier transforms. For example

$$G(\omega) = \int_{-\infty}^{\infty} G(t)exp(-\iota wt)\, d\omega. \qquad (16)$$

Similar relationships can be derived for the Fourier transforms of other variables. Substitution of Eq. (14) in Eq. (9) and using Eqs. (6) and (15) gives the following result

$$G(\omega) = 1/M(\omega_0^2-\omega^2), \qquad (17)$$

where

$$\omega_0 = \sqrt{(\phi/M)}, \qquad (18)$$

is the natural frequency of the spring. Equation (17) gives the desired GF in the frequency space. The GF in the time space can then be calculated from Eq. (14). Finally, we obtain by using Eqs. (11) - (15)

$$u(\omega) = G(\omega)f(\omega). \qquad (19)$$

Equation (19) along with Eq. (13) yields Eq. (11), the desired particular solution of Eq. (5). The solution can also be written directly from Eq. (19) by taking the following convolution

$$u(t) = \int G(t-t')\, f(t')\, dt'. \qquad (20)$$

In a general case, the temporal GF **G**(t) is to be defined as retarded or advanced GF for positive and negative times to account for causality [3]. The causal GFs that we consider in this chapter, must obey the causality condition that the response cannot precede the cause. Hence

$G(t) = 0$ for $t < 0$. (21)

Since $G(\omega)$ has a singularity on the real axis (Eq. (17)), one has to take an appropriate contour for the integration to ensure causality.

For positive values, the variable ω can be identified as the frequency. In Eqs. (12)- (14) we have used the same symbol for the functions and its Fourier transform for notational brevity, the identifying feature being the functional dependence on t or ω.

The above derivation gives the basic features of the GF method. Although the example was rather trivial, it does bring out some of the main characteristics of the GF that are summarized below:

i. GF is an operator being the inverse of an operator as defined by Eq. (9). We need a representation for calculating the GF. Fourier representation is one such representation and other representations are possible. The choice of a representation depends upon the physical conditions to be simulated.

ii. GF is linear so the solutions are additive as can be verified from Eq. (20). It is, however, possible to include nonlinear effects in the probe.

iii. GF has poles at the natural frequencies of the system. These poles can be identified as resonances.

iv. GF is a characteristic of the system and is independent of the probe.

v. Once the GF is known, it can be used to obtain the solution (or the response) to any probe by using Eq. (20).

vi. The static GF is the zero frequency limit of the dynamic GF and is independent of the mass of the particles.

3. Discrete lattice model of a solid

In this section we describe the main features of the lattice model of a solid that accounts for its discrete atomistic structure explicitly. We will include only those features that are directly relevant to the GF method. For details please consult any text book on solid state physics or lattice dynamics such as the excellent classics by Kittel [17], Born and Huang [18], or Maradudin et al. [3]. In this section we shall consider only a general 3D lattice. The special case of two-dimensional (2D) graphene will be discussed in Sec. 5.

An important input to all the lattice calculations is the interatomic potential. All atomistic defect calculations are based upon minimizing the free enthalpy of the solid that consists of an ionic part which gives the elastic contribution, and an electronic part. These are, of course, coupled. When a defect such as a vacancy is introduced in the lattice, the relaxed configuration depends upon the charge states of the defect [19]. The same applies to extended defects like a quantum dot or a quantum well. A rigorous calculation of the relaxed configuration would require an *ab intio* quantum mechanical modeling of the coupled ion-electron system in the whole lattice. Such calculations are limited to very small model crystallites consisting of only a few hundred atoms [20]. At the other extreme is the continuum model, in which the electron effects are totally neglected. The

continuum model reproduces the bulk mechanical characteristics of the defect and has been extensively used for a long time. It has the advantage of computational convenience but obviously has a limited validity.

The intermediate approach is to use models in which the effect of the electrons is included in an empirical and phenomenological manner by using an effective interatomic potential [21, 22], [23], [24, 25] [26] . This approximation has been has been used in almost all lattice-statics/lattice-dynamics/molecular-dynamics defect calculations. See, for example, the review article by Stangl *et al.* [27] and the monographs by Harrison [28] and Bimberg *et al.* [29] for application of phenomenological potentials to semiconductors. Such model potentials have been used in many atomistic calculations in Ge/Si and other semiconductors using MD. See, for example, the papers by Makeev and Madhukar [30], and Swadener *et al.* [31], which also give other references.

As discussed by Harrison [28], the inherent assumptions in all these calculations are: (i) tight binding approximation which allows us to treat atoms as separate entities, (ii) adiabatic approximation which assumes that the electrons respond adiabatically to the ionic displacements, and (iii) the independent electron approximation. These assumptions result into a separation of the crystal Hamiltonian into a part that corresponds to ionic interactions and another part that gives the energy of the electrons. Of course the ionic interactions are also affected by the electrons. This contribution is included in a parametric model potential. Such models [21, 22, 24, 25, 31-34], [26] give correct values for many observable parameters including the energy of vacancies and other defects, which lends credence to the validity of the model potential. The potentials [21, 22, 24, 25,

32] to which we refer in this paper belong to this class of models. Some other potentials are available in the literature [33, 35-39], which all have comparable advantages. We have used the Tersoff potential for some applications to graphene because of its computational convenience. It reproduces the correct energy of the defect and has been widely used in defect calculations on covalent solids.

The GF method described in this chapter is based upon the Born von Karman (BvK) model [3, 17, 18] of a lattice. This model fully accounts for the discrete structure of the lattice. The basic assumptions of the BvK model are:

i. Adiabatic approximation: As described above, it implies that the contribution of the electrons to the crystal Hamiltonian is additive. We therefore consider only the ionic interactions in the lattice model. The electronic energies can be calculated separately and added to the ionic energies to obtain the total energy of the crystal.

ii. Cyclic boundary conditions: The whole crystal is assumed to be divided in identical supercells. This enables us to neglect the surface effects in a model lattice. This is, therefore, applicable only to large crystals in the regions far away from the surfaces. This assumption is obviously not valid for nanocrystals. In such cases the surfaces are modeled as defects in the ideal BvK lattice.

iii. Harmonic approximation: The atomic displacements are assumed to be small enough such that their cubic and higher powers can be neglected in potential energy of the crystal.

iv. Equilibrium and stability: The crystal is assumed to be in equilibrium in the absence of external forces so there is no net force at any atom in the lattice.

The lattice structure of a solid can be described in terms of its primitive real-space lattice vectors of the Bravais lattice and the corresponding reciprocal lattice vectors (see, for example, [17]). The primitive lattice vectors define a unit cell. Each unit cell may contain one or more atoms. We consider a 3D lattice containing N unit cells with each unit cell containing p atoms. So the total number of degrees of freedom in our model are 3pN corresponding to 3 coordinates of pN atoms.

We assume a Cartesian frame of reference with the axes parallel to the crystallographic axes and its origin at a lattice site. The Z axis is assumed to be normal to the plane of the paper. We denote the lattice sites of the origin of the unit cells by the indices L, L', etc., and the Cartesian coordinates x,y, and z by indices α, β, γ, etc.. The atoms inside each unit cell are labeled by the index κ. The atom at the origin of each unit cell is labeled as $\kappa=0$ and other atoms as $\kappa=1,2,$ p-1. In all the cases considered in this paper p is either 1 or 2. For example for a monoatomic Bravais lattice such as fcc Cu or Au, p=1. For semiconductors such as Si or Ge that have a diamond lattice structure, and for 2D graphene, p=2.

We can label each atom by the index doublet Lκ and write its position vector as follows:

$$\mathbf{R}(L\kappa) = \mathbf{R}(L0) + \mathbf{r}(\kappa), \qquad (22)$$

where **R**(L) is the position vector of the origin of the L^{th} unit cell and **r**(κ) is the position vector of the κ^{th} atom relative to the origin of its own unit cell. At equilibrium each atom is assumed to be located at its lattice site and the energy at equilibrium is assumed to be zero.

We now introduce lattice distortion and denote the displacement of the atom Lκ by **u**(Lκ). In time dependent problems, u(Lκ) will also depend upon t and its Fourier transform over time will depend upon the frequency ω. However, for brevity of notation, we will not show the explicit dependence of u(Lκ) on t or ω unless locally needed to avoid confusion.

We write the potential energy of the lattice in the form of a Taylor series as follows

$$W=-\Sigma_{L\kappa\alpha}\, f_\alpha(L\kappa)u_\alpha(L\kappa)+(1/2)\Sigma_{L\kappa\alpha}\Sigma_{L'\kappa'\beta}\, \phi_{\alpha\beta}(L\kappa,L'\kappa')u_\alpha(L\kappa)u_\beta(L'\kappa'), \quad (23)$$

where **-f** and **ϕ** are the Taylor coefficients. They are defined by

$$f_\alpha(L\kappa) = -\partial W/\partial u_\alpha(L\kappa), \quad (24)$$

and

$$\phi_{\alpha\beta}(L\kappa,L'\kappa') = \partial^2 W/\partial u_\alpha(L\kappa)\partial u_\beta(L\kappa'), \qquad (25)$$

where the derivatives are evaluated at zero displacement. To clarify the notation, **f**(Lκ) is a 3D vector which denotes the force at the atom Lκ. Its three Cartesian components are denoted by $f_\alpha(L\kappa)$ where α =x,y, or z. Similarly **ϕ**(Lκ,L'κ') is a 3x3 matrix which is called the force- constant matrix between atoms at Lκ and L'κ'**.** Its 9 elements are denoted by $\phi_{\alpha\beta}(L\kappa,L'\kappa')$ for α, β = x,y, or z.

The force and the force-constant matrices can be obtained from the interatomic potential [3]. These matrices must obey the constraints imposed by the translation and rotation symmetry of the lattice, which determine the number of independent elements in the matrices [3]. In addition, the equilibrium condition of zero net force on the solid imposes the following constraints:

i. For all α

$$\Sigma_{L\kappa} f_\alpha(L\kappa) = 0, \qquad (26)$$

ii. For all L, κ, α, and β

$$\Sigma_{L'\kappa'} \phi_{\alpha\beta}(L\kappa,L'\kappa') = 0. \qquad (27)$$

At equilibrium W must be minimum. By minimizing the right-hand side (RHS) of Eq. (23), we obtain the following equation for the displacements

$$f_\alpha(L\kappa) = \Sigma_{L'\kappa'\beta}\, \phi_{\alpha\beta}(L\kappa,L'\kappa')u_\beta(L'\kappa'), \qquad (28)$$

Equation (28) is the generalized form of Eq. (2) for a many particle system in which **f** is the probe and u is the response. For time dependent problems, the Newtonian term has to be added to Eq. (28) as in Eq. (4). For a finite system one can write a set of coupled equations for pN atoms as in Eq. (28) and solve it numerically for all u. This is essentially the technique used in MD. As mentioned in Sec. 1, solving Eq. (28) directly may become computationally too expensive for large N – say a few million or billion atoms. As we shall see in this section, the GF method offers a computationally efficient method for solving Eq. (28).

Using Eqs. (23) and (28) we can write the equation of motion for the atom Lκ for a perfect lattice as follows:

$$M(L\kappa)\partial^2 u(L\kappa)/\partial t^2 = f_\alpha(L\kappa) - \sum_{L'\kappa'\beta} \phi_{\alpha\beta}(L\kappa, L'\kappa')u_\beta(L'\kappa'). \qquad (29)$$

For modeling of phonons, we take the Fourier transform of the displacement over time as given in Eq. (13). This will make **u**(Lκ) a function of the frequency ω, which can be identified as the phonon frequency. The nonlinear terms in the potential, if any, will add terms on the right of Eq. (29) that will depend upon u. Alternatively, the nonlinear effects can be included by treating **f** and **ϕ** as functions of **u** and hence t**.** In the harmonic approximation, **f** and **ϕ** are independent of **u** and t. Further, in the harmonic approximation phonon frequencies are independent of **f**. If **f** is nonzero, the equilibrium

location of atoms will change and they will simply vibrate about their new position of equilibrium.

We define the discrete Fourier transform over space of the displacement vector as follows

$$u_\alpha(L\kappa) = (1/N)\sum_k u_\alpha(\mathbf{k};\kappa) \exp[\imath \mathbf{k}.\mathbf{R}(L\kappa)], \qquad (30)$$

where **k** is a vector in the reciprocal space of the lattice. The number of allowed **k** vectors in the first Brillouin zone is N equal to the number of unit cells in a supercell. For notational brevity, we follow the common convention and denote the matrix in real space and the Fourier (reciprocal) space by the same symbol. The distinguishing feature between the two is that the functional dependence on **k** will be shown explicitly for a matrix in reciprocal space. An equation similar to Eq. (30) can be written down for the force vector defined by Eq. (24). Instead of Eq. (30), an alternative definition of the Fourier transform has also been used in the literature in which **R**(L0) is used in the exponent instead of **R**(Lκ). The two definitions differ only by a phase factor exp[ι**k**.**r**(κ)].

Because of the orthogonality of the reciprocal and the direct-lattice vectors, the vector **k** can take only certain allowed discrete values [3, 4] and can be confined to the first Brillouin zone of the lattice. The inverse Fourier transform of Eq. (30) can be obtained by using the following relation [3]

$$\sum_L \exp[\imath \mathbf{k}.\mathbf{R}(L0)] = \delta_d(\mathbf{k}), \qquad (31)$$

and

$$\Sigma_k \exp[\iota \mathbf{k}.\mathbf{R}(L0)] = \delta_d(L), \qquad (32)$$

where δ_d is the discrete analogue of the Dirac delta function defined by Eq. (10). It is 0 for non zero value of the argument and equal to N if the argument is 0. Strictly speaking the sum in Eq. (31) is equal to N not just for **k**=0 but whenever **k** is equal to a reciprocal lattice vector. However, in this paper, we will be concerned with only those cases when **k** is restricted to the first Brillouin zone of the lattice.

Using Eqs. (31) and (32) in Eq. (30), we find the following equation for the inverse transform of the displacement vector

$$u_\alpha(\mathbf{k};\kappa) = \Sigma_L\, u_\alpha(L\kappa) \exp[-\iota \mathbf{k}.\mathbf{R}(L\kappa)]. \qquad (33)$$

Note the absence of the factor (1/N) in Eq. (33) as compared to Eq. (30) .

The above equations are valid for a perfect lattice as well as a lattice containing defects. A perfect infinite lattice or a perfect lattice with periodic boundary conditions has full translation symmetry. This combined with the condition of invariance of the potential energy against rigid body translations leads to the following additional constraints [3]:

i. The Taylor coefficient $f_\alpha(L\kappa) = 0$ for all $L\kappa$. Physically this condition implies that for a perfect lattice in equilibrium without any external forces, there cannot be any force on

any lattice site. Of course if external forces are applied, then **f** can represent the applied external forces.

ii. The force-constant matrix $\phi_{\alpha\beta}(L\kappa,L'\kappa')$ depends upon L and L' only through their difference. This is a consequence of translation symmetry. Since all atoms on one sublattice are equivalent, any atom can be chosen as the origin. The force-constant matrix can therefore be labeled by a single index as $\phi_{\alpha\beta}(0\kappa,L\kappa')$ that gives the force constant between any two atoms for which the unit cells are separated by $\mathbf{R}(L\kappa') - \mathbf{R}(0\kappa)$. This enables us to write the force-constant matrix in terms of its discrete Fourier transform as defined below:

$$\phi_{\alpha\beta}(0\kappa,L\kappa') = (1/N)\sum_{\mathbf{k}} \phi_{\alpha\beta}(\mathbf{k};\kappa,\kappa') \exp[\imath\mathbf{k}.\{\mathbf{R}(L\kappa')-\mathbf{R}(0\kappa)\}], \qquad (34)$$

where $\boldsymbol{\phi}(\mathbf{k})$ is the Fourier transform of the force-constant matrix. Its matrix elements are $\phi_{\alpha\beta}(\mathbf{k};\kappa,\kappa')$. As in Eq. (33), the inverse transform of $\boldsymbol{\phi}(\mathbf{k})$ is given by $\boldsymbol{\phi}$

$$\phi_{\alpha\beta}(\mathbf{k};\kappa,\kappa') = \sum_{L} \phi_{\alpha\beta}(0\kappa,L\kappa') \exp[-\imath\mathbf{k}.\{\mathbf{R}(L\kappa')-\mathbf{R}(0\kappa)\}]. \qquad (35)$$

Since κ and κ' can take p values, the matrix $\boldsymbol{\phi}(\mathbf{k})$ is 3px3p square matrix. By generalizing the derivation given in Sec. 2 to 3d many particle systems, it can be shown that the phonon frequencies ω are the eigenvalues of the dynamical matrix [3, 18] defined in terms of $\boldsymbol{\phi}(\mathbf{k})$ as follows

$$D_{\alpha\beta}(\mathbf{k};\kappa,\kappa') = (M_\kappa M_{\kappa'})^{-1/2}\, \phi_{\alpha\beta}(\mathbf{k};\kappa,\kappa'), \qquad (36)$$

where M_κ is the mass of the atom κ. In view of the translation symmetry in a perfect lattice for which Eq. (36) is valid, M_κ is independent of L. The dynamical matrix $\mathbf{D}(\mathbf{k})$ is used extensively in the lattice dynamical calculations. Lattice statics for static problems is independent of the atomic masses. The relevant matrix for lattice statics is $\boldsymbol{\phi}(\mathbf{k})$. [40]

The matrices $\mathbf{D}(\mathbf{k})$ and $\boldsymbol{\phi}(\mathbf{k})$ have 3p eigenvalues. From Eq. (36), their eigen values are related through a factor depending upon the atomic masses. By using Eq. (27) it can be shown that the determinant of $\mathbf{D}(\mathbf{k})$ is zero at k=0 and at least three of its eigenvalues vary as k^2 near k =0 for a normal 3D solid. These are called the acoustic modes. The remaining 3p-3 eigenvalues are, in general, finite at k=0 and are called the optical modes.

4. Lattice statics Green's function

First we consider a perfect lattice. The phonon GF of the lattice is defined as follows [3]:

$$\mathbf{G}(\mathbf{k},\omega^2) = [-\omega^2\mathbf{I} + \boldsymbol{\phi}(\mathbf{k})]^{-1}, \qquad (37)$$

where $\mathbf{I}$ is the unit matrix. In steady state the displacements are independent of time so the steady state corresponds to ω=0. We define the lattice statics Green's function (LSGF) as the zero frequency limit of the phonon GF [4]. In the Fourier k-space, the LSGF is given by :

$$\mathbf{G}(\mathbf{k}) = [\boldsymbol{\phi}(\mathbf{k})]^{-1}. \qquad (38)$$

Since the determinant of $\boldsymbol{\phi}(\mathbf{k})$ is zero at k=0, $\mathbf{G}(\mathbf{k})$ is singular at k=0, which is consistent with the discussion in Sec. 2. Analogous to $\boldsymbol{\phi}(\mathbf{k})$, the matrix elements of the 3px3p matrix $\mathbf{G}(\mathbf{k})$ are labeled as $G_{\alpha\beta}(\mathbf{k};\kappa,\kappa')$. The LSGF in the real space is defined by its inverse Fourier transform in analogy with Eq. (34) as follows

$$G_{\alpha\beta}(0\kappa,L\kappa') = (1/N)\sum_{\mathbf{k}} G_{\alpha\beta}(\mathbf{k};\kappa,\kappa') \exp[\imath\mathbf{k}.\{\mathbf{R}(L\kappa')-\mathbf{R}(0\kappa)\}]. \quad (39)$$

Equation (39) provides a convenient and computationally efficient semi-analytic representation for calculation of the LSGF. For a solid containing N atoms, it requires inversion of only 3p x 3p matrices. In most cases of practical interest as considered here, p is a small number, i.e. 1 or 2.

For real space calculations, it is convenient to define a 3pNx3pN vector space in terms of the three coordinates of the pN atoms. In this representation we denote the real-space force constant and the GF matrices by $\boldsymbol{\Phi}$ and $\boldsymbol{\Gamma}$ respectively. These matrices will be 3pNx3pN square matrices and their matrix elements are $\phi_{\alpha\beta}(L\kappa,L'\kappa')$ and $G_{\alpha\beta}(L\kappa,L'\kappa')$ respectively. Similarly, in the same vector space, we define 3pN dimensional column matrices $\mathbf{U}$ and $\mathbf{F}$ for the displacement and the force vectors with matrix elements $U_{\alpha}(L\kappa)$ and $f_{\alpha}(L\kappa)$ respectively. Using Eq. (38) it can be easily shown that in this representation

$$\boldsymbol{\Gamma} = \boldsymbol{\Phi}^{-1}. \quad (40)$$

In the same representation, Eq. (23) can be written in the following compact form $\boldsymbol{\Gamma}$

$$W = -\mathbf{F}.\mathbf{U} + (1/2)\mathbf{U}^{T}.\mathbf{\Phi}.\mathbf{U} \qquad (41)$$

If defects are introduced in the lattice then its translation symmetry is broken. Consequently, even in the absence of any external force, **f** becomes non zero for at least some L and κ [4]. Further, ϕ and **G** depend upon L and L' separately and not merely on their difference [3]. Hence it is not possible to define their Fourier transform in terms of a single vector **k** as in Eqs. (34) and (39). In such cases, the defect LSGF, the GF for the lattice with defects, is calculated as follows [4], [41].

We denote the force constant matrix for the defective lattice and the defect LSGF by $\mathbf{\Phi}^*$ and $\mathbf{\Gamma}^*$ respectively. In the representation of lattice sites, $\mathbf{\Gamma}^*$ and $\mathbf{\Phi}^*$ are 3Np x 3Np matrices. The GF is formally given by as in Eq. (40)

$$\mathbf{\Gamma}^* = [\mathbf{\Phi}^*]^{-1}. \qquad (42)$$

We write

$$\mathbf{\Phi}^* = \mathbf{\Phi} - \Delta\mathbf{\Phi}, \qquad (43)$$

where $\Delta\mathbf{\Phi}$ denotes the change in the force-constant matrix $\mathbf{\Phi}$ caused by the defect(s). From (40), (42) and (43), we obtain the following equation

$$\boldsymbol{\Gamma^* = \Gamma + \Gamma\, \Delta\Phi\, \Gamma^*.} \qquad (44)$$

Equation (44) is the Dyson equation for calculation of the defect GF. This equation shows that in order to calculate **G***, we have to first define a reference state and calculate **G** and the corresponding **ΔΦ**. The change **ΔΦ** is obtained by the interatomic potential between the defect and the host atoms. In quantum mechanical problems, **ΔΦ** gives the change in the system Hamiltonian. Methods for solving the Dyson equation have been discussed in detail in references [3] [4, 42].

In the present case we have taken the perfect lattice with full translation symmetry as the reference state. In practice, any state can be chosen to be the reference state for which **G** can be calculated and **ΔΦ** can be conveniently defined [42-44]. Further, although **G** for the reference state is calculated using the harmonic or the linear approximation, **ΔΦ** can include non-linear terms [45, 46].

For a defect lattice, Eq. (41) is modified as follows:

$$W^* = -\mathbf{F}.\mathbf{U} + (1/2)\, \mathbf{U}^T.\boldsymbol{\Phi}^*.\mathbf{U}, \qquad (45)$$

where **U** and **F** are now identified as the displacement and the force vectors in the defect lattice. The solution of Eq. (45) gives the displacement field:

$$\mathbf{U = \Gamma^*\, F.} \qquad (46)$$

A very useful form of Eq. (46) has been derived in [4]. It is shown that Eq. (46) is exactly equivalent to

$$\mathbf{U} = \mathbf{\Gamma}\ \mathbf{F^*}, \qquad (47)$$

where

$$\mathbf{F^*} = \mathbf{F} + \Delta\mathbf{\Phi}\ \mathbf{U}. \qquad (48)$$

Equations (46) or (47) are the main equations of the LSGF method. They are used to calculate the atomic displacements, which give the lattice distortion or the lattice relaxation caused by the defect. In this method the defect is characterized by $\Delta\mathbf{\Phi}$. Equation (46) gives the displacement in terms of the defect GF and the forces on the atoms at the lattice sites of the reference state. Equation (47), the alternative form of Eq. (46), gives the displacement in terms of the perfect-lattice GF and an effective force denoted by **F***, as defined by Eq. (48).

The effective force **F*** is called the Kanzaki force [4]. From Eq. (48), we can identify it as the force due to the defect on the relaxed lattice sites, in contrast to **F,** that denotes the force at the original lattice site.

5. Multiscale Green's function

The LSGF method provides a convenient and computationally efficient mathematical technique for multiscale modeling of nanomaterials. We need multiscale models of nanomaterials for bridging length scales as well as temporal scales. In this section we will

discuss only the length scales. The problem of multi-time scales will be discussed in the next section.

The coupling between the lattice and the continuum models in the GF method is achieved by using the Born's method of long waves [18]. This method establishes the correspondence between the force constants and the elastic constants. Using the Born's method, it has been shown in [4] that the LSGF varies as 1/R for large R and reduces asymptotically to the continuum GF (CGF) for 3D lattices. The case of 2D graphene is, however, different and will be described in Sec. 7.

To establish the correspondence between the LSGF and CGF, we make **R(Lκ)** and **k** continuous variables and replace the summation in Eq. (39) by integration over the reciprocal space. In conformity with the continuum model notation, we replace **R(Lκ)** by the continuous variable **x** for large R(Lκ), and the discrete wave vector **k** by the continuous wave vector **q**, which spans all space from -∞ to ∞.

$$\mathbf{G(x)} \cong (1/2\pi)^3 \int \mathbf{G(q)} \exp(\iota \mathbf{q.x})\, \mathbf{dq}, \qquad (49)$$

We obtain the asymptotic limit of **G(x)** by using Duffin's lemma (see, for example, [4]). In the limit $x \to \infty$, smaller values of q make more significant contribution to the integral in Eq. (49). Accordingly, we expand **G(q)** in powers of q as given below.

$$\mathrm{Lim}_{q\to 0}\, \mathbf{G(q)} = \mathrm{Lim}_{q\to 0}\, [\phi(\mathbf{q})]^{-1} \qquad (50)$$

For low values of q, $\phi(\mathbf{q})$ has the following behavior [3] for the acoustic modes

$$\phi(q) \sim O(q^2) + O(q^4). \qquad (51)$$

Using the expansion given in Eq. (51), in Eq. (50), we can carry out the integral in Eq. (49) term by term which gives the asymptotic expansion of the LSGF.

The leading term in $\boldsymbol{\phi}(\mathbf{q})$ as $q \to 0$ is the q^2 term. This term is identical to the Christoffel matrix in the continuum model. Keeping only this term, we can show [4] that

$$\mathrm{Lim}_{q\to 0}\, \mathbf{G(q)} = \mathrm{Lim}_{q\to 0}\, [\boldsymbol{\phi}(\mathbf{q})]^{-1} = [\boldsymbol{\Lambda}(\mathbf{q})]^{-1}, \qquad (52)$$

where $\boldsymbol{\Lambda}$ is the well-known Christoffel matrix of the continuum model [5], which is defined in terms of **c**, the elastic constant tensor, as follows

$$\Lambda_{ij}(\mathbf{q}) = c_{ikjl}\, q_k\, q_l, \qquad (53)$$

and i,j,k,l are Cartesian components in the continuum model. Summation over repeated Cartesian indices is assumed. The CGF $\mathbf{G_c(q)}$ in q space is defined as the Christoffel matrix. Thus we get

$$\mathrm{Lim}_{q\to 0}\, \mathbf{G(q)} = \mathbf{G_c(q)} = [\boldsymbol{\Lambda}(\mathbf{q})]^{-1} = O(1/q^2) \qquad (54)$$

In view of Eq. (54), the integrand in Eq (49) has a $1/q^2$ singularity at q = 0. It is integrated out in 3D because the integral element in 3D is proportional to q^2. It can be shown [4] that the integral is proportional to 1/|x| which is the continuum GF in 3D. The subscript c

on **G** in Eq. (49) denotes the GF for the continuum model. It has been extensively used in modeling solids using the boundary element analysis. It provides a powerful technique for solving the boundary value problems for solids with and without defects. See, for example, [47], [48], [49], [50].

It is important to note that the asymptotic relation given by Eq. (49) is valid only for the perfect lattice GF **G**. It is generally not valid for the defect GF **G*** defined by Eq. (44) unless the term containing $\Delta\Phi$ is negligible [51]. In most cases of practical interest it is not negligible. For example, in the case of a vacancy $\Delta\Phi = \Phi$. Moreover, if the effect of $\Delta\Phi$ is negligible, then the information about the defect is lost. Calculations in this region are therefore not of interest for studying the properties of the defect.

The advantage of writing the displacement in the form of Eq. (47) is now obvious. We can use the full power of continuum mechanics by using the continuum-model GF for **G** where needed while retaining the discrete lattice effects and all the characteristics of the defect exactly in **F***.

Equation (47) is the master equation of our MSGF method. The displacement of the atom at Lκ, which is a matrix element of **U** is given by $_{\beta}$

$$u_\alpha(L\kappa) = \sum_{L'\kappa'\beta} G_{\alpha\beta}(L\kappa,L'\kappa')f^*_\beta(L'\kappa') \qquad (55)$$

where **f*** is the Kanzaki force given which is the corresponding matrix element of **F*** given by Eq. (48) . For Lκ close to the defect we use **G** to be the LSGF, whereas for large

values $|\mathbf{R(L\kappa) - R(L'\kappa')}|$ we choose $\mathbf{G} = \mathbf{G_c}$, the CGF. Since $\mathbf{G_c}$ is the asymptotic limit of G for large $|\mathbf{R(L\kappa) - R(L'\kappa')}|$, the linkage is seamless.

It must be emphasized that even with G_c, we use the discrete lattice value of **f* (**or **F*)** as defined by Eq. (48) near the defect in terms of **ΔΦ.** The Kanzaki force retains all the characteristics of the defect through **ΔΦ**. Thus Eq. (55) is the multiscale representation of the lattice distortion or strains due to the defect since it relates the discrete lattice parameters through **f*** to the continuum model parameters through $\mathbf{G_c}$.

The advantage of writing the displacement in the form of Eq. (47) is now obvious. We can use the full power of the continuum mechanics by using the continuum-model GF G_c for **G** where needed, while retaining the discrete lattice effects and all the characteristics of the defect exactly in **F***.

Further, nonlinear effects associated with the defect host interaction can be incorporated in the MSGF method through **ΔΦ** while still retaining the linear simplicity of the GFs. A convenient technique for including nonlinear effects is to calculate the atomic displacements in a zone near the defect by using MD and use these values to calculate **f***. MD accounts for the nonlinear forces. The displacements outside the zone are then calculated by using Eq. (55) by using LSGF or CGF for **G** depending upon the value of $|\mathbf{R(L\kappa) - R(L'\kappa')}|$. This method has been applied to model realistic size Ge quantum dots in Si and Au islands in Cu [45, 46]. A somewhat different version of the MSGF method has been applied to quantum nanostructures in semiconductors [44, 52].

One important advantage of the MSGF method is that the continuum parameters like strain and stresses are uniquely defined in this method. In a pure discrete lattice model, the atomic displacements are defined at discrete lattice points. In many applications, one needs elastic strains which are also measured experimentally. Strain is a continuum parameter defined in terms of the derivatives of the displacement field and cannot be defined as such for discrete values of the displacements. In practice, one has to assume some averaging scheme in order to define the derivatives. Although elegant techniques [53] have been developed for this purpose, the averaging process is not unique and requires careful attention to various conservation laws. In the MSGF method, the variable x in Eq. (49) is continuous so the derivatives of **u** with respect to x are uniquely defined.

6. Causal Green's function for temporal modeling

We have developed a new temporal modeling technique [11] by incorporating causal GF in MD. We refer to this method as the GFMD method. At least in some idealized cases, it has been shown that GFMD can model time scales over 6-9 orders of magnitude at the atomistic level. So far this technique has been applied to only a few idealized cases but it clearly has the potential for a much wider and realistic applications in all physical, chemical, and biological systems where MD is used.

In a certain class of problems in which atoms vibrate about an equilibrium site, GFMD gives exact results in the harmonic approximation. Even for nonlinear vibrational problems, GFMD has been shown to accelerate the MD by up to 8 orders of magnitude [11]. This enables modeling processes up to microseconds. Examples of such problems are phonon transport, thermal conduction etc.. In problems involving itinerant atoms,

such as diffusion or crystal growth, GFMD should also be able to accelerate MD substantially.

The GFMD method has been described in detail in [11]. Here we will only quote the highlights of the technique given in [11]. Consider the equation of motion for the atom Lκ as given by Eq. (29). The symbols in this section will have a slightly more general meaning. The time dependent displacement and the velocity vectors of the atom Lκ will be denoted by **u**(Lκ,t) and **c**(Lκ,t), respectively. We assume that at time t=0, **u**(Lκ,0) and **f** (Lκ) denote the values of displacement and force for the atom Lκ. As in classical MD, we need to solve the following equation for **u**:

$$\begin{aligned} M_{L\kappa}\frac{\partial^2 u_\alpha(L\kappa,t)}{\partial t^2} &= -\frac{\partial W}{\partial u_\alpha(L\kappa,t)} \\ &= f_\alpha(L\kappa) - \sum_{L'\beta}\phi_{\alpha\beta}(L\kappa,L'\kappa')u_\beta(L'\kappa',t) + \Delta f_\alpha(L\kappa), \end{aligned} \tag{56}$$

where $\Delta\mathbf{f}$ represents higher than harmonic terms in the expansion of W. This term depends upon **u** and hence on t.

As in Eq. (45), we define 3pN dimensional vectors **U**(t), **C**(t), **F**, and Δ**F**(t), and 3pN x 3pN matrices **Φ** and **D**. However, in the present time dependent case, for brevity of notation, their elements are denoted by the corresponding lower case quantities weighted with atomic masses. For example, the (α,Lκ) element of **U**(t) is $\sqrt{M_{L\kappa}}u_\alpha(L\kappa,t)$ and of **F** is $(1/\sqrt{M_{L\kappa}})f_\alpha(L\kappa)$. The formal solution of equation (56) in the operator form is then given by

$$\mathbf{U}(t) = \left(\mathbf{I}\frac{\partial^2}{\partial t^2} - \mathbf{D} \right)^{-1} \mathbf{F}_{\text{eff}}(t), \qquad (57)$$

where **I** is the unit matrix, **M** is a diagonal matrix with atomic masses as its elements,

$$\mathbf{D} = \mathbf{M}^{-1/2}\mathbf{\Phi}\mathbf{M}^{-1/2}, \qquad (58)$$

and

$$\mathbf{F}_{\text{eff}}(t) = \mathbf{F} + \Delta\mathbf{F}(t). \qquad (59)$$

The inverse operator in Eq. (57) is the GF. We solve Eq. (57) by using Laplace transform that gives the causal GF [3], which is 0 for t<0, to ensure causality. Using the numerical approximation $\mathbf{F}_{\text{eff}}(t) = \mathbf{F}$, we obtain the exact result [11]:

$$\mathbf{U}(t) = \mathbf{V}\mathbf{U}^*(t), \qquad (60)$$

Where (proof error: add negative sign in the first term)

$$U_i^*(t) = (F_i^* / E_i^2)[\cos(E_i t) - H(t)] + (C_{0i}^* / E_i)\sin(E_i t) + U_{0i}^* \cos(E_i t), \qquad (61)$$

$\mathbf{U}^*$, $\mathbf{F}^*$, $\mathbf{C}_0^*$, and $\mathbf{U}_0^*$ are $\mathbf{V}^T(\mathbf{U}, \mathbf{F}, \mathbf{C}_0$, and $\mathbf{U}_0)$ respectively, **V** is the matrix of eigenvectors of **D**, E_i (i=1..3pN) is an eigenvalue of **D**, and H(t) is the Heaviside step function, which is 0 for t <0, and 1 for t>0.

Equation (60) can be used as stated for phonons in systems where the harmonic approximation is valid but the analytical lattice dynamics cannot be used due to lack of translational symmetry. To account for anharmonic effects in a multiparticle system, we use the MD type iterative approach. We expand W locally at each time step. We calculate $\mathbf{U}(t)$ from equation (60) in steps of Δt. We keep Δt small so that $\Delta\mathbf{F}(t)$ is negligible at each step. This introduces a constraint on the step size Δt, which is much less severe than that in the conventional MD.

The convergence of GFMD is much faster than MD because in the basic MD only the first term on the right of Eq. (56) is retained whereas GFMD retains up to quadratic terms in the expansion of W, and the GFMD gives an exact solution of the temporal equation for any value of t. The constraint on t or Δt arises because of the necessity to keep $\Delta\mathbf{F}(t)$ small. The basic MD can of course be accelerated somewhat by using more refined numerical techniques that partly account for the second order terms by iteration.

We can compare the convergence of the GFMD and the MD techniques by estimating the errors in the two techniques as follows. We denote the displacement variable in the expansion of W in Eq. (23) by ξ. Suppose the actual normalized value of a displacement is unity which we calculate in S_{MD} steps in the MD and S_{GFMD} in the GFMD technique. Then $\xi_{MD} = 1/S_{MD}$ for MD and $1/S_{GFMD}$ for GFMD. In the conventional MD second and higher powers of ξ_{MD} are neglected so the error in each step is of the order of $(\xi_{MD})^2$. The corresponding error in GFMD is $(\xi_{GFMD})^3$. For MD to be at least as accurate as GFMD, we must have

$$(\xi_{MD})^2 = (\xi_{GFMD})^3 \qquad (62)$$

or

$$S_{MD} \approx (S_{GFMD})^{3/2}. \qquad (63)$$

Considering that in practical cases $S_{GFMD} \approx 10^6$, Eq. (63) shows that number of iterations needed in the conventional MD to attain the same accuracy as the GFMD technique is more by a factor of 1000.

Finally, we remark that the GFMD technique is particularly efficient for modeling of phonons and elastic properties of nanomaterials. This is because it is specifically the u^2 term in Eq. (23) that defines the phonon and elastic response of a solid [3]. This term is exactly included in the GFMD technique. In the conventional MD the u^2 term is included only through additional iterations that is a relatively inefficient process.

7. Application to 2D graphene

As we have seen in Sec 5, a multiscale model of a solid can be constructed if we can establish a correspondence between its lattice and continuum GFs. Such a correspondence has been rigorously proved for normal 3D solids in Sec 5. Unfortunately, that does not apply to 2D graphene or any solid that is strictly 2D. The reason for this discrepancy will be apparent from Eq. (49). The integration volume element is proportional to q^2 in 3D, which integrates out the q^2 singularity at q=0. The corresponding element in 2D is proportional to q. Hence the singularity in the integral

survives as 1/q. This is responsible for the long-range logarithmic behavior of the GF and size effect in the static as well as dynamic response of graphene [54, 55].

However, it is still possible to set up a correspondence between lattice and continuum models for a 2D graphene film in deflection mode. The displacement field in the deflection mode is normal to the plane of graphene. For small displacements, in the harmonic approximation, the out-of-plane displacements are not coupled with the in-plane displacements. Consequently, the GF for the deflection mode is a scalar. Moreover, the q^2 term in Eq. (51) is identically zero [55] in the deflection mode for graphene. Hence the leading term in $\phi(q)$ in the deflection mode is $O(q^4)$ for graphene.

The integral for the $O(q^4)$ term in Eq. (49) can be carried out analytically. This shows that the continuum limit of the LSGF of a graphene sheet in the deflection mode, corresponds to the GF for an elastically stable Kirchhoff plate but not the GF for two-dimensional Christoffel equations. This correspondence demonstrates the mechanical stability of graphene in deflection and is necessary for relating its mechanical parameters to its lattice parameters. Using this approach, an explicit expression has been derived [55-57] for relating the continuum flexural rigidity to the force constants of graphene. This relationship can be used to measure flexural rigidity of graphene directly from experimentally observed phonon dispersion. However, a more rigorous calculation or measurement of rigidity will involve some more contributions

Now we consider the force constants for graphene that are the most important parameters for the lattice GFs. For multiscale applications, force constants give the elastic constants. This relation ensures that the LSGF is seamlessly linked with the CGF. The force

constants can be obtained from the interatomic potential. A popular choice of potential for graphene is the Tersoff potential and its variations. This potential, which is essentially a bond-order potential, extends up to second neighbor distances. It is convenient for MD simulations and has been used for calculations of strains, friction, and many other physical characteristics of graphene [58-64] and many more solids.

The second neighbor Tersoff type potential does not seem to be a good choice for phonon calculations and those properties of graphene that are sensitive to details of the phonon spectrum. An optimized Tersoff Brenner potential seems to be more suitable for modeling of phonons in graphene [65]. The main point is that to obtain a good fit between the calculated and the experimental values of the phonon dispersion for graphene, interatomic interactions have to be included at least up to fourth neighbor atoms [66], [56, 57, 67, 68]. However, if only the harmonic GF is needed, a detailed knowledge of the potential is not required. The force constants can be obtained by parametric fitting [3] of the calculated phonon dispersion with measured values.

For phonon applications, we give the 3 x 3 force constant matrices for graphene as defined by Eq. (25). A graphene unit cell contains two non-equivalent atoms C1 and C2 as shown in Fig. 2. This figure also shows the nearest neighbors of C1 and C2. All these atoms are in the plane of the graphene lattice. The force constants depend upon the choice of coordinate axes, which is shown in Fig. 2. The Z axis is assumed to be normal to the plane of graphene.

We denote a lattice site $L\kappa$ by its 2D position vector $\mathbf{l}$, where l_x and l_y are its x and y coordinates, respectively. The coordinates of the atoms are given in the units of a where

2a = distance between C1 and A2 is the lattice constant. The Z-coordinate of each atom in Fig 2 is zero. The force constant matrices $\boldsymbol{\phi}(0;\mathbf{l})$ between C1 and its first four nearest neighbors identified by different values of $\mathbf{l}$ are written below. The form of the matrices is most general for the hexagonal symmetry of graphene:

$$\boldsymbol{\phi}(0;2s,0) = -\begin{pmatrix} \alpha_1 & 0 & 0 \\ 0 & \beta_1 & 0 \\ 0 & 0 & \delta_1 \end{pmatrix}, \tag{64}$$

$$\boldsymbol{\phi}(0;0,2) = -\begin{pmatrix} \alpha_2 & \gamma_2 & 0 \\ -\gamma_2 & \beta_2 & 0 \\ 0 & 0 & \delta_2 \end{pmatrix}, \tag{65}$$

$$\boldsymbol{\phi}(0;-4s,0) = -\begin{pmatrix} \alpha_3 & 0 & 0 \\ 0 & \beta_3 & 0 \\ 0 & 0 & \delta_3 \end{pmatrix}, \tag{66}$$

$$\phi(0;5s,1) = -\begin{pmatrix} \alpha_4 & \gamma_4 & 0 \\ \gamma_4 & \beta_4 & 0 \\ 0 & 0 & \delta_4 \end{pmatrix}, \qquad (67)$$

where $s=1/\sqrt{3}$. The form of the force constant matrices between C1 and other atoms in the same neighbor shell and also between C2 and its neighbors can be obtained from symmetry. Note that the matrix elements corresponding to xz and yz are 0 for each atom. This shows that the displacements in the plane of the lattice are not coupled with the out-of-plane displacements. This decoupling is valid only in the harmonic approximation.

In the multiscale method based upon Born's method of long waves as described in Sec 5, we compare the phonon frequencies with the frequencies given by the Christoffel matrix as in Eq. (51). This yields the following relations between the force constants and the elastic constants for graphene:

$$c11 = C_u [2\alpha_1^2 + \alpha_1(6\alpha_2 + 19\alpha_3 + 35\alpha_4 + 54\alpha_5 + 6\beta_1 + 18\beta_2 + 3\beta_3 + 33\beta_4 + 18\beta_5 +$$

$$14\sqrt{3}\,\gamma_4) + \alpha_2(6\alpha_3 + 12\alpha_4 + 6\beta_1 + 6\beta_3 + 12\beta_4) + 8\alpha_3^2 + \alpha_3(83\alpha_4 + 54\alpha_5 +$$

$$9\beta_1 + 18\beta_2 + 24\beta_3 + 21\beta_4 + 18\beta_5 + 2\sqrt{3}\,\gamma_4) + 53\alpha_4^2 + \alpha_4(108\alpha_5 + 51\beta_1 +$$

$$36\beta_2 + 27\beta_3 + 162\beta_4 + 36\beta_5 + 40\sqrt{3}\,\gamma_4) + \alpha_5(54\beta_1 + 54\beta_3 + 108\beta_4) +$$

$$\beta_1(18\beta_2 + 9\beta_3 + 9\beta_4 + 18\beta_5 + 6\sqrt{3}\,\gamma_4) + \beta_2(18\beta_3 + 36\beta_4) + \beta_3(45\beta_4 +$$

$$18\beta_5 + 18\sqrt{3}\,\gamma_4) + 9\beta_4^2 + 36\beta_4\,\beta_5 - 12\,\gamma_4^2], \qquad (68)$$

$$c66 = C_u\,[2\beta_1^2 + \beta_1(6\beta_2 + 19\beta_3 + 35\beta_4 + 54\beta_5 + 6\alpha_1 + 18\alpha_2 + 3\alpha_3 + 33\alpha_4 + 18\alpha_5 -$$

$$14\sqrt{3}\,\gamma_4) + \beta_2(6\beta_3 + 12\beta_4 + 6\alpha_1 + 6\alpha_3 + 12\alpha_4) + 8\beta_3^2 + \beta_3(83\beta_4 + 54\beta_5 +$$

$$9\alpha_1 + 18\alpha_2 + 24\alpha_3 + 21\alpha_4 + 18\alpha_5 - 2\sqrt{3}\,\gamma_4) + 53\beta_4^2 + \beta_4(108\beta_5 + 51\alpha_1 +$$

$$36\alpha_2 + 27\alpha_3 + 162\alpha_4 + 36\alpha_5 - 40\sqrt{3}\,\gamma_4) + \beta_5(54\alpha_1 + 54\alpha_3 + 108\alpha_4) +$$

$$\alpha_1(18\alpha_2 + 9\alpha_3 + 9\alpha_4 + 18\alpha_5 - 6\sqrt{3}\,\gamma_4) + \alpha_2(18\alpha_3 + 36\alpha_4) + \alpha_3(45\alpha_4 +$$

$$18\alpha_5 - 18\sqrt{3}\,\gamma_4) + 9\alpha_4^2 + 36\alpha_4\,\alpha_5 - 12\,\gamma_4^2], \qquad (69)$$

where

$$C_u = 1/[4c\sqrt{3}(\alpha_1 + \alpha_3 + 2\alpha_4 + \beta_1 + \beta_3 + 2\beta_4)], \qquad (70)$$

and c = 3.355 Angstrom is the interplanar separation in graphite and 2a=2.462 is the lattice constant of graphene. In deriving the above equations, we have used the fact that the volume per atom is equal to $a^2c\sqrt{3}$.

The values of the force constants reported in [57] were derived from the interatomic potential reported in that paper. Unfortunately, the potential is incorrect and actually unstable [56]. However, the values of the force constants given in that paper are correct in the sense that they can be treated as independent parameters for fitting the phonon

dispersion relations. The force constants certainly give an excellent agreement between the calculated and the observed dispersion curves [57]. Of course they are related only with the derivatives of the potential at equilibrium lattice sites and are not meant to give the detailed interatomic potential.

The values of the force constants are given below in N/m:

$\alpha_1 = 409.705; \beta_1 = 145.012; \delta_1 = 98.920;$

$\alpha_2 = -40.8; \beta_2 = 74.223; \gamma_2 = -9.11; \delta_2 = -8.191$

$\alpha_3 = -33.203; \beta_3 = 50.10; \delta_3 = 5.802;$

$\alpha_4 = 10.539; \beta_4 = 4.993; \gamma_4 = 2.184; \delta_4 = -5.213.$ (71)

The values of the two elastic constants calculated by using Eqs. (68) and (69) are: c11= 1060 GPa and c66=440 GPa, which fit exactly with the experimental values for graphite given by Blakslee et al [69]. Because the interplanar interaction in graphite is much weaker than the intaplanar interactions, c11 and c66 of graphene should be approximately equal to those for graphite.

Using the method described earlier in this section, the flexural rigidity of graphene for the present fourth neighbor interaction model is given by the following expression[57] :

$D = -(\sqrt{3}/36)(\delta_1+18\delta_2 + 16\delta_3 + 98\delta_4 + 162\delta_5)a^2 = 2.13$ eV. (72)

This value is in the range of values as reported in the literature [70, 71]. There is some confusion in the literature about the actual value of the rigidity and a wide range of values have been reported. In any case, the derivation as given here, shows that the rigidity is very sensitive to the range of the interatomic potential: the farther neighbors contribute more than the nearer neighbors. The rigidity may also be size dependent. Hence it is difficult to assess the validity of the calculated value.

Finally, we quote the result [11] obtained by using GFMD method for propagation of elastic pulses or ripples in graphene. Propagation of pulses is an important characteristic of a material and is useful in understanding its elastic response and phonon transport. Such a calculation for a finite lattice cannot be done analytically even in the harmonic approximation.

The model used in [11] is particularly simple and only serves the purpose of illustration. The origin and the system of axes is same as given in Fig. 2. The model consists of about 1100 carbon atoms located at the equilibrium graphene lattice sites at time t=0. As in [55], the outer atoms within the second neighbor distance of the outermost vibrating atoms are constrained so that their displacement is zero at all times. The size of the active lattice along the X-axis is about 5.52 nm. Propagation is initiated by imposing an initial displacement d in the Z direction on the central atom.

We consider only the atomic displacements in the Z direction. Only the Z components f_z, Δf_z, and ϕ_{zz} in Eq. (56) contribute to these displacement. To account for the anharmonic effects in the Z direction, the MD type iterative approach is used. The quantities f_z and ϕ_{zz}

are calculated for each atom at each time step. These components change at each step due to anharmonicity. A major approximation in these calculations is that the displacements in the Z direction and in the XY plane are not coupled. This is strictly valid only in the harmonic approximation. It is, therefore, to keep d small so that the coupling between the ZZ and the planar components of ϕ can be neglected at all times. In these calculation d was taken to be 0.01a and the results are normalized to this initial value.

The results are illustrated in Fig. 3, which shows a snapshot of the ripples or the instantaneous displacements of all atoms in the lattice at about 20 microseconds. It is important to realize that, as stated earlier, the GFMD approach described here can reproduce the rippling dynamics of graphene in the case of infinitesimally small displacements. At sufficiently high lattice temperatures, however, it is expected that the long-wavelength flexural modes [16] will be significantly suppressed (private communication from Dr Alex Smolyanitsky).

An important test of the numerical convergence of the model is the invariance of the total energy of the system at all times. It was found that change in the energy of the system at each time step was less than 10^{-4} per cent. This shows that the results had converged even up to microseconds and GFMD has extended and bridged the time scales at least in this model problem by 8 orders of magnitude - from femto to microseconds.

In the basic MD the lack of energy conservation results in an increase of the crystal temperature. This necessitates quenching of temperature that may introduce errors in the displacements. This problem should be substantially reduced in the GFMD calculations

since the energy is very well conserved. An additional advantage of the GFMD is that the same formulation can be used to bridge the length scales by taking the asymptotic limit of the static part of the GF as described in Sec 5.

8. Conclusions and future work

The MSGF and the GFMD techniques are computationally very efficient and the next step is to combine them into a unified technique that can be applied to static as well as dynamic problems. These techniques have so far been applied to only symmetric lattices. They need to be developed for unsymmetric, disordered, and finite systems like amorphous solids, polymers, and liquids. One interesting application in which these techniques will be useful is model plasmonics in graphene that is sensitive to mechanical strains [72]. One reason why the MSGF and the GFMD techniques are not very widespread is the lack of efficient software. It would be useful, therefore, to develop efficient and freely available software for these techniques.

Finally, the GFMD technique should be useful for solving time-dependent problems that are very difficult to solve by using existing methods. So far this technique has been applied only to an idealized case of graphene. This technique should be applicable to modeling of time-dependent processes in various physical, chemical, and bio systems for which presently which MD is used. In particular, this technique should be useful in simulation of protein folding and unfolding which has been of great interest for many years [73].

Acknowledgements: The author thanks Drs. Lauren Rast, David Read, and Alex Smolyanitsky for helpful discussions.

References

1. Morse, P.M. and Feshbach, H., *Methods of Theoretical Physics*. I ed. Vol. 1. 1953, New York: McGraw-Hill Publishing Company. 1939.

2. Barton, G., *Elements of Green's Functions and Propagation*. 1989, Oxford: Clarendon Press

3. Maradudin, A.A., Montroll, E.W., Weiss, G.H., and Ipatova, I.P., *Theory of lattice dynamics in the harmonic approximation*. 2 ed. Solid State Physics, ed. H. Ehrenreich, F. Seitz, and D. Turnbull. Vol. Supp 3. 1971, New York: Academic Press.

4. Tewary, V.K. (1973) 'Green-Function Method for Lattice Statics' Advances in Physics, **22**, 757-810

5. Ting, T.C.T., *Anisotropic Elasticity: Theory and Applications*. 1996, New York: Oxford University Press.

6. Puzder, A., Williamson, A.J., Reboredo, F.A., and Galli, G. (2003) 'Structural stability and optical properties of nanomaterials with reconstructed surfaces' Physical Review Letters, **91** 157405

7. Hirth, J.P. and Lothe, J., *Theory of dislocations*. Second ed. 1992, Florida: Krieger Publishing Company.

8. Gibson, J.B., Goland, A.N., Milgram, M., and Vineyard, G.H. (1960) 'DYNAMICS OF RADIATION DAMAGE' Physical Review, **120**, 1229-1253

9. Rapaport, D.C., *The art of molecular dynamics simulation*. Second ed. 2004, Cambridge, UK: Cambridge University Press.

10. Voter, A.F., Montalenti, F. and Germann, T.C. (2002) 'Extending the time scale in atomistic simulation of materials' Annual Review of Materials Research, **32**, 321-346

11. Tewary, V.K. (2009) 'Extending the time scale in molecular dynamics simulations: Propagation of ripples in graphene' Physical Review B, **80**

12. Geim, A.K. and Novoselov, K.S. (2007) 'The rise of graphene' Nature Materials, **6**, 183-191

13. Novoselov, K.S., Fal'ko, V.I., Colombo, L., Gellert, P.R., Schwab, M.G., and Kim, K. (2012) 'A roadmap for graphene' Nature, **490**, 192-200

14. Novoselov, K.S., Jiang, D., Schedin, F., Booth, T.J., Khotkevich, V.V., Morozov, S.V., and Geim, A.K. (2005) 'Two-dimensional atomic crystals' Proceedings of the National Academy of Sciences of the United States of America, **102**, 10451-10453

15. Mas-Balleste, R., Gomez-Navarro, C., Gomez-Herrero, J., and Zamora, F. (2011) '2D materials: to graphene and beyond' Nanoscale, **3**, 20-30

16. Fasolino, A., Los, J.H. and Katsnelson, M.I. (2007) 'Intrinsic ripples in graphene' Nature Materials, **6**, 858-861

17. Kittel, C., *Introduction to Solid State Physics*. 7 ed. 1996, New York: John Wiley.

18. Born, M. and Huang, K., *Dynamical Properties of Crystal Lattices*. 1954, London: Oxford University Press.

19. Lannoo, M. and Bourgoin, J., *Point Defects in Semiconductors I*. Springer Series in Solid-State Sciences. Vol. 22. 1981, New York: Springer Verlag.

20. Parr, R.G. and Yang, W., *Density-functional theory of atoms and molecules*. International Series of Monographs on Chemistry, ed. R. Breslow, et al. 1989, Oxford: Oxford Science Publications.

21. Tersoff, J. (1989) 'Modeling Solid-State Chemistry - Interatomic Potentials for Multicomponent Systems' Physical Review B, **39**, 5566-5568

22. Tersoff, J. (1988) 'Empirical Interatomic Potential for Silicon with Improved Elastic Properties' Physical Review B, **38**, 9902-9905

23. Brenner, D.W., Shenderova, O.A., Areshkin, D.A., Schall, J.D., and Frankland, S.J.V. (2002) 'Atomic modeling of carbon-based nanostructures as a tool for developing new materials and technologies' CMES-Computer Modeling in Engineering & Sciences, **3**, 643-673

24. Baskes, M.I. (1997) 'Determination of modified embedded atom method parameters for nickel' Materials Chemistry and Physics, **50**, 152-158

25. Baskes, M.I. (1992) 'Modified Embedded-Atom Potentials for Cubic Materials and Impurities' Physical Review B, **46**, 2727-2742

26. Tewary, V.K. (2011) 'Phenomenological interatomic potentials for silicon, germanium and their binary alloy' Physics Letters A, **375**, 3811-3816

27. Stangl, J., Holy, V. and Bauer, G. (2004) 'Structural properties of self-organized semiconductor nanostructures' Reviews of Modern Physics, **76**, 725-783

28. Harrison, P., *Quantum Wells, Wires, and Dots: Theoretical and Computaional Physics*. 2002, New York: John Wiley.

29. Bimberg, D., Grundmann, M. and Ledentsov, N., *Quantum Dot Heterostructures*. 1999: John Wiley, New York.

30. Makeev, M.A. and Madhukar, A. (2001) 'Simulations of atomic level stresses in systems of buried Ge/Si islands' Physical Review Letters, **86**, 5542-5545

31. Swadener, J.G., Baskes, M.I. and Nastasi, M. (2005) 'Stress-induced platelet formation in silicon: A molecular dynamics study' Physical Review B, **72** 201202

32. Cleri, F. and Rosato, V. (1993) 'Tight-Binding Potentials for Transition-Metals and Alloys' Physical Review B, **48**, 22-33

33. Balamane, H., Halicioglu, T. and Tiller, W.A. (1992) 'Comparative-Study of Silicon Empirical Interatomic Potentials' Physical Review B, **46**, 2250-2279

34. Tersoff, J., Teichert, C. and Lagally, M.G. (1996) 'Self-organization in growth of quantum dot superlattices' Physical Review Letters, **76**, 1675-1678

35. Cai, W.S., Lin, Y. and Shao, X.G. (2005) 'Interatomic potential function in cluster research' Progress in Chemistry, **17**, 588-596

36. Cheng, D., Huang, S. and Wang, W. (2005) 'The structure of 55-atom Cu-Au bimetallic clusters: Monte Carlo study' European Physical Journal D, **39**, 41-48

37. Mishin, Y., Sorensen, M.R. and Voter, A.F. (2001) 'Calculation of point-defect entropy in metals' Philosophical Magazine a-Physics of Condensed Matter Structure Defects and Mechanical Properties, **81**, 2591-2612

38. Yavari, A., Ortiz, M. and Bhattacharya, K. (2007) 'A theory of anharmonic lattice statics for analysis of defective crystals' Journal of Elasticity, **86**, 41-83

39. Zhigilei, L.V. and Dongare, A.M. (2002) 'Multiscale modeling of laser ablation: Applications to nanotechnology' CMES-Computer Modeling in Engineering & Sciences, **3**, 539-555

40. Andreev, A.D., Downes, J.R., Faux, D.A., and O'Reilly, E.P. (1999) 'Strain distributions in quantum dots of arbitrary shape' Journal of Applied Physics, **86**, 297-305

41. Thomson, R., Zhou, S.J., Carlsson, A.E., and Tewary, V.K. (1992) 'Lattice Imperfections Studied by Use of Lattice Green-Functions' Physical Review B, **46**, 10613-10622

42. Yang, B. and Tewary, V.K. (2004) 'Continuum Dyson's equation and defect Green's function in a heterogeneous anisotropic solid' Mechanics Research Communications, **31**, 405-414

43. Yang, B. and Tewary, V.K. (2006) 'Efficient Green's function modeling of line and surface defects in multilayered anisotropic elastic and piezoelectric materials' CMES-Computer Modeling in Engineering & Sciences, **15**, 165-177

44. Yang, B. and Tewary, V.K. (2005) 'Green's function-based multiscale modeling of defects in a semi-infinite silicon substrate' International Journal of Solids and Structures, **42**, 4722-4737

45. Read, D.T. and Tewary, V.K. (2007) 'Multiscale model of near-spherical germanium quantum dots in silicon' Nanotechnology, **18** 105402

46. Tewary, V.K. and Read, D.T. (2004) 'Integrated Green's function molecular dynamics method for multiscale modeling of nanostructures: Application to Au nanoisland in Cu' CMES-Computer Modeling in Engineering & Sciences, **6**, 359-371

47. Pan, E. (2002) 'Mindlin's problem for an anisotropic piezoelectric half-space with general boundary conditions' Proceedings of the Royal Society of London Series a-Mathematical Physical and Engineering Sciences, **458**, 181-208

48. Yang, B. and Tewary, V.K. (2003) 'Formation of a surface quantum dot near laterally and vertically neighboring dots' Physical Review B, **68**, 6

49. Tewary, V.K. (2004) 'Elastostatic Green's function for advanced materials subject to surface loading' Journal of Engineering Mathematics, **49**, 289-304

50. Berger, J.R. and Tewary, V.K. (2001) 'Greens functions for boundary element analysis of anisotropic bimaterials' Engineering Analysis with Boundary Elements, **25**, 279-288

51. Tewary, V.K. (2004) 'Multiscale Green's-function method for modeling point defects and extended defects in anisotropic solids: Application to a vacancy and free surface in copper' Physical Review B, **69**, 13

52. Yang, B. and Tewary, V.K. (2007) 'Multiscale modeling of point defects in Si-Ge(001) quantum wells' Physical Review B, **75** 144103

53. Cormier, J., Rickman, J.M. and Delph, T.J. (2001) 'Stress calculation in atomistic simulations of perfect and imperfect solids' Journal of Applied Physics, **89**, 99-104

54. Tewary, V.K. and Yang, B. (2009) 'Singular behavior of the Debye-Waller factor of graphene' Physical Review B, **79** 125416

55. Yang, B. and Tewary, V.K. (2008) 'Multiscale Green's function for the deflection of graphene lattice' Physical Review B, **77** 245442

56. Tewary, V.K. and Yang, B. (2010) 'Parametric interatomic potential for graphene (vol 79, 075442, 2009)' Physical Review B, **81**

57. Tewary, V.K. and Yang, B. (2009) 'Parametric interatomic potential for graphene' Physical Review B, **79** 075442

58. Deng, Z., Smolyanitsky, A., Li, Q.Y., Feng, X.Q., and Cannara, R.J. (2012) 'Adhesion-dependent negative friction coefficient on chemically modified graphite at the nanoscale' Nature Materials, **11**, 1032-1037

59. Smolyanitsky, A. and Killgore, J.P. (2012) 'Anomalous friction in suspended graphene' Physical Review B, **86** 125432

60. Smolyanitsky, A., Killgore, J.P. and Tewary, V.K. (2012) 'Effect of elastic deformation on frictional properties of few-layer graphene' Physical Review B, **85** 035412

61. Smolyanitsky, A. and Tewary, V.K. (2013) 'Manipulation of graphene's dynamic ripples by local harmonic out-of-plane excitation' Nanotechnology, **24** 055701

62. Smolyanitsky, A. and Tewary, V.K. (2011) 'Simulation of lattice strain due to a CNT-metal interface' Nanotechnology, **22** 085703

63. Smolyanitsky, A. and Tewary, V.K. (2011) 'Atomistic simulation of a graphene-nanoribbon-metal interconnect' Journal of Physics-Condensed Matter, **23** 355006

64. Smolyanitsky, A., Zhu, S.Z., Deng, Z., Li, T., and Cannara, R.J. (2014) 'Effects of surface compliance and relaxation on the frictional properties of lamellar materials' Rsc Advances, **4**, 26721-26728

65. Lindsay, L. and Broido, D.A. (2010) 'Optimized Tersoff and Brenner empirical potential parameters for lattice dynamics and phonon thermal transport in carbon nanotubes and graphene' Physical Review B, **81** 205441

66. Wirtz, L. and Rubio, A. (2004) 'The phonon dispersion of graphite revisited' Solid State Communications, **131**, 141-152

67. Zimmermann, J., Pavone, P. and Cuniberti, G. (2008) 'Vibrational modes and low-temperature thermal properties of graphene and carbon nanotubes: Minimal force-constant model' Physical Review B, **78** 104426

68. Mohr, M., Maultzsch, J., Dobardzic, E., Reich, S., Milosevic, I., Damnjanovic, M., Bosak, A., Krisch, M., and Thomsen, C. (2007) 'Phonon dispersion of graphite by inelastic x-ray scattering' Physical Review B, **76** 035439

69. Blakslee, O.L., Proctor, D.G., Seldin, E.J., Spence, G.B., and Weng, T. (1970) 'Elastic Constants of Compression-Annealed Pyrolytic Graphite' Journal of Applied Physics, **41**, 3373

70. Lindahl, N., Midtvedt, D., Svensson, J., Nerushev, O.A., Lindvall, N., Isacsson, A., and Campbell, E.E.B. (2012) 'Determination of the Bending Rigidity of Graphene via Electrostatic Actuation of Buckled Membranes' Nano Letters, **12**, 3526-3531

71. Wei, Y.J., Wang, B.L., Wu, J.T., Yang, R.G., and Dunn, M.L. (2013) 'Bending Rigidity and Gaussian Bending Stiffness of Single-Layered Graphene' Nano Letters, **13**, 26-30

72. Rast, L., Sullivan, T.J. and Tewary, V.K. (2013) 'Stratified graphene/noble metal systems for low-loss plasmonics applications' Physical Review B, **87** 045428

73. Shea, J.E. and Brooks, C.L. (2001) 'From folding theories to folding proteins: A review and assessment of simulation studies of protein folding and unfolding' Annual Review of Physical Chemistry, **52**, 499-535

Figure Captions

Fig. 1: A particle attached to a spring. F is the applied force and u is the displacement of the particle.

Fig. 2- The bond structure of hexagonal graphene and the coordinate axes. The dots show the lattice sites occupied by carbon atoms A1,B1,C1,A2,B2, and C2. The origin of coordinates is at C1.

Fig. 3: Snapshot of normalized atomic displacements in graphene at about 20 microseconds. Coordinates X and Y are in units of half lattice constant.

Figure 1

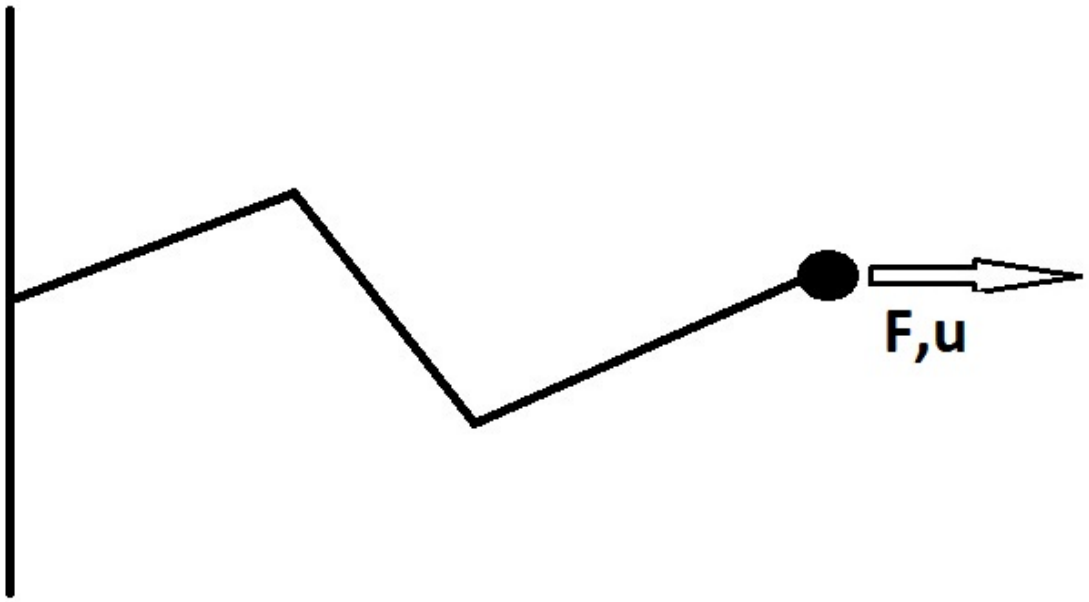

Figure 2

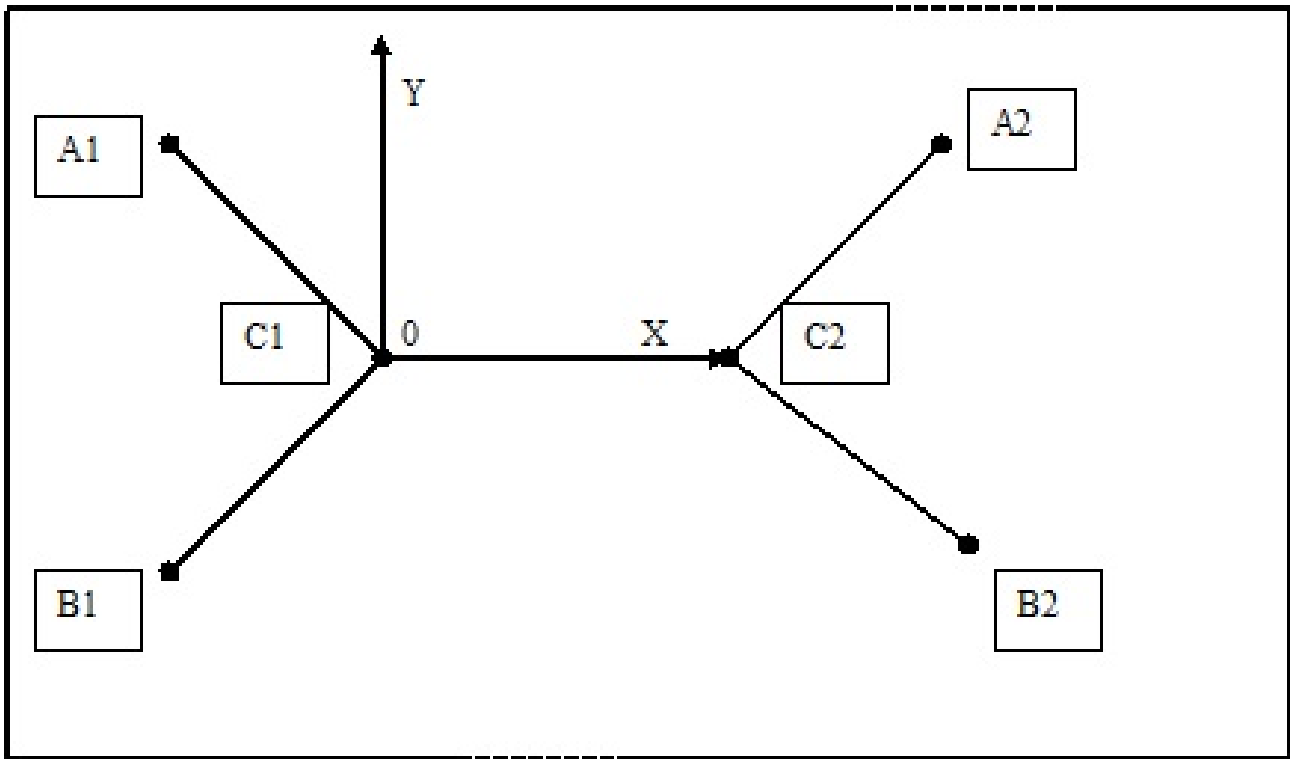

Figure 3

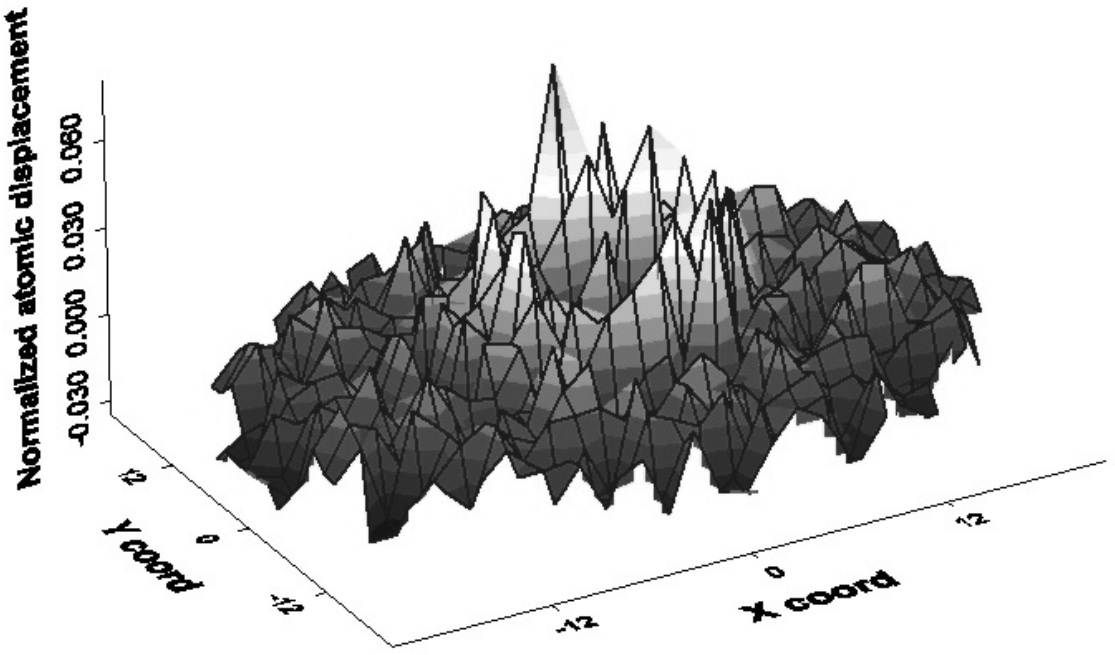
Normalized atomic displacement
-0.030
0.000
0.030
0.060
Y coord
12
0
-12
X coord
-12
0
12